JOURNAL OF GEOPHYSICAL RESEARCH, VOL. 113, A02101, doi:10.1029/2007JA012582, 2008

Inversion solutions of the elliptic cone model for disk frontside full halo coronal mass ejections

X. P. Zhao[1]

Received 4 June 2007; revised 30 July 2007; accepted 10 October 2007; published 8 February 2008.

[1] A new algorithm is developed for inverting six unknown elliptic cone model parameters from five observed CME halo parameters. It is shown that the halo parameter α includes the information on the coronal mass ejection (CME) propagation direction denoted by two model parameters. On the basis of the given halo parameter α, two approaches are presented to find out the CME propagation direction. The two-point approach uses two values of α observed simultaneously by COR1 and COR2 on board STEREO A and B. The one-point approach combines the value of α with such simultaneous observation as the location of CME-associated flare, which includes the information associated with CME propagation direction. Model validation experiments show that the CME propagation direction can be accurately determined using the two-point approach, and the other four model parameters can also be well inverted, especially when the projection angle is greater than 60°. The propagation direction and other four model parameters obtained using the one-point approach for six disk frontside full halo CMEs appear to be acceptable, though the final conclusion on its validation should be made after STEREO data are available.

Citation: Zhao, X. P. (2008), Inversion solutions of the elliptic cone model for disk frontside full halo coronal mass ejections, *J. Geophys. Res.*, *113*, A02101, doi:10.1029/2007JA012582.

1. Introduction

[2] Coronal mass ejections (CMEs) with an apparent (sky-plane) angular width of 360° are called full halo CMEs, and frontside full halo CMEs (FFH CMEs) if there are near-surface activities associated with the full halo CMEs. FFH CMEs with associated flares occurring within 45° and beyond 45° but within 90° from the solar disk center are called, respectively, disk and limb FFH CMEs [*Gopalswamy et al.*, 2003]. Disk FFH CMEs are mostly symmetric and ellipse-like. Limb FFH CMEs are, however, often asymmetric, including ragged structures as well as the smooth structure. The ragged structures are believed to be formed by the interaction between super-Alfvenic shocks and preexisting coronal streamers and rays [*Sheeley et al.*, 2000]. This paper focus on the inversion solution of the elliptic cone model for disk FFH CMEs.

[3] Disk FFH CMEs have been shown to be the most geoeffective kind of solar events. The geoeffectiveness rate of total disk FFH CMEs between 1997 and 2005 reaches 75% [*Gopalswamy et al.*, 2007], supporting the earlier result of 71% obtained using the disk FFH CMEs between 1997 and 2000 [*Zhao and Webb*, 2003]. It is the higher end of the range of geoeffectiveness rate of solar activities. To predict when and in what percentage a disk FFH CME could generate intense geostorms, we need to determine when and which part of the huge interplanetary counterpart (ICME) of the disk FFH CME could hit Earth's magnetosphere. It requires the knowledge of the size, shape, propagation direction and speed of ICMEs. However, coronagraphs record only the total content of free electrons in CMEs along the line of sight. A 2-D disk FFH CME cannot unambiguously provide any real geometrical and kinematic properties of a 3-D CME.

[4] CMEs are believed to be driven by free magnetic energy stored in field-aligned electric currents, and before eruption, the metastable structure with free magnetic energy is confined by overlying arched field lines. The magnetic configuration of most, if not all, CMEs is thus expected to be magnetic flux ropes with two ends anchored on the solar surface [e.g., *Riley et al.*, 2006], and the outer boundary of the top (or leading) part of the ropes may be approximated by an ellipse with its major axis aligned with the orientation of the ropes.

[5] Most limb CMEs appear as planar looplike transients with a radially pointed central axis and a constant angular width. The existence of halo CMEs implies that the looplike transients are three-dimensional. Both looplike and halolike CMEs show the evidence of the rope-like magnetized plasma structure of CMEs. A conical shell (or cone) model, i.e., a hollow body which narrows to a point from a round, flat base, was suggested to qualitatively understand the formation of some full halo CMEs [*Howard et al.*, 1982].

[6] The cone model, as a proxy of the rope-like magnetized plasma structure of CMEs, has been used to produce modeled elliptic halos, and the model parameters that are used to produce the modeled halos can be determined by

[1]W. W. Hansen Experimental Physics Laboratory, Stanford University, Stanford, California, USA.

0148-0227/08/2007JA012582$09.00

matching modeled halos to observed halos [*Zhao et al.*, 2002]. The three model parameters of the circular cone model can also be directly inverted from three halo parameters that characterize 2-D elliptic halos [*Xie et al.*, 2004].

[7] The geometrical and kinematical properties obtained using the circular cone model for the 12 May 1997 disk FFH CME [*Zhao et al.*, 2002] were introduced at the boundary of a 3-D MHD solar wind model [*Odstrcil and Pizzo*, 1999], and the associated ICME near the Earth's orbit were successfully reproduced [*Odstrcil et al.*, 2004]. It indicates that the idea for using cone-like geometric model to invert model parameters from halo parameters is valid and useful in estimating the real geometrical and kinematical properties for disk FFH CMEs.

[8] It was found that the circular cone model can be used to reproduce only a limited cases of halo CMEs, and that the elliptic cone model, i.e., a body which narrows to an apex from an elliptic, flat base, would be better than the circular cone model in approximating the rope-like CMEs [*Zhao*, 2005; *Cremades and Bothmer*, 2005]. However, the inversion solution of the elliptic cone model obtained using the approaches of both *Zhao* [2005] and *Cremades and Bothmer* [2005] are often not unique.

[9] In what follows we first define five halo parameters and three halo types for disk FFH CMEs in section 2. We then develop a new elliptic cone model with six model parameters, and produce modeled halos that are expected to be observed by multi-spacecraft, such as STEREO A, SOHO, and STEREO B in section 3. The inversion equation system of the elliptic cone model and the expressions of its solution are established in section 4. On the basis of two-point and one-point observations of CMEs, two approaches are presented in section 5 for determining the CME propagation direction and other model parameters, and the model validation experiment is carried out to see whether or not the established inversion equation system and the two approaches are acceptable and useful. Finally we summarize and discuss the results in section 6.

2. Description and Classification of Observed Elliptic Halos

[10] Figure 1 displays six disk FFH CMEs selected from Table 3 of *Cremades* [2005]. The onset date of the six events is shown on the top of each panel.

2.1. Five Halo Parameters: D_{se}, α, SA_{xh}, SA_{yh}, and ψ

[11] The white oval curve in each panel of Figure 1 is obtained by fitting to five selected points along the outer edge of each CME halo (see *Cremades* [2005] for details). All white curves are ellipses and occur on the sky-plane Y_hZ_h where Y_h and Z_h are the axes of the heliocentric ecliptic coordinate system, pointing to the west and north, respectively.

[12] As shown in each panel, the short thick green line, D_{se}, denotes the distance between the solar disk center and the elliptic halo center, and axes X'_c and Y'_c are aligned with and perpendicular to D_{se}, respectively. The location of elliptic halos on the sky-plane can be specified using parameter D_{se} and the angle α between axes X'_c and Y_h. The shape and size of elliptic halos can be specified using two semi-axes of the halos, SA_{xh} and SA_{yh}, where SA_{xh} and SA_{yh} are located near the axes X'_c and Y'_c, respectively. The orientation of elliptic halos can thus be specified by the angle ψ between X'_c and SA_{xh} or Y'_c and SA_{yh}.

[13] The five halo parameters, SA_{xh}, SA_{yh}, D_{se}, α and ψ, can be measured once the outer edge of halo CMEs is recognized. The top of each panel in Figure 1 shows the measured values of the five halo parameters for each event.

2.2. Halo Equations

[14] By using four halo parameters SA_{xh}, SA_{yh}, D_{se}, and ψ, a 2-D elliptic halo on the plane $X'_cY'_c$ can be expressed

$$\begin{bmatrix} x'_c \\ y'_c \end{bmatrix} = \begin{bmatrix} D_{se} \\ 0 \end{bmatrix} + \begin{bmatrix} \cos\psi & \sin\psi \\ -\sin\psi & \cos\psi \end{bmatrix} \begin{bmatrix} x_{eh} \\ y_{eh} \end{bmatrix} \tag{1}$$

where

$$\begin{bmatrix} x_{eh} \\ y_{eh} \end{bmatrix} = \begin{bmatrix} SA_{xh}\sin\delta_h \\ SA_{yh}\cos\delta_h \end{bmatrix} \tag{2}$$

The symbol δ_h in equation (2) is the angle of radii of elliptic halos relative to SA_{yh} axis, and increases clockwise along an elliptic rim from 0° to 360°.

[15] The halo observed in the sky-plane Y_hZ_h can be obtained by rotating an angle of α as follows

$$\begin{bmatrix} y_h \\ z_h \end{bmatrix} = \begin{bmatrix} \cos\alpha & \sin\alpha \\ -\sin\alpha & \cos\alpha \end{bmatrix} \begin{bmatrix} x'_c \\ y'_c \end{bmatrix} \tag{3}$$

2.3. Three Types of Observed Halos

[16] It has been shown that the semi minor (major) axis of the elliptic halos formed by the circular cone model must be aligned with X'_c (Y'_c) axis. In other words, the halo parameter ψ must be equal to zero (see *Xie et al.* [2004] and *Zhao et al.* [2002, Figure 2] for details). Because of the uncertainty in identifying elliptic halos from coronagraph CME images, we consider SA_{xh} being nearly aligned with X'_c if $|\psi| < 10°$.

[17] Figure 1 shows that the halo parameter ψ that characterizes the orientation of elliptic halos can be any value between −45° and 45°. It means that the semi major (or minor) axis can be located anywhere on the plane of $X'_cY'_c$. This fact suggests that most of disk FFH CMEs cannot be fitted or inverted using the circular cone model.

[18] To distinguish the halos that may be inverted using the circular cone model from the halos that can be inverted using the elliptic cone model, we classify the observed elliptic halos into the following three types:

$$\text{Type A} : |\psi| < 10°, SA_{xh} < SA_{yh};$$

$$\text{Type B} : |\psi| < 10°, SA_{xh} \geq SA_{yh};$$

$$\text{Type C} : 10° \leq |\psi| \leq 45°.$$

[19] The top left panel of Figure 1 shows a sample of Type A halo where SA_{xh} denotes the semi minor axis and is

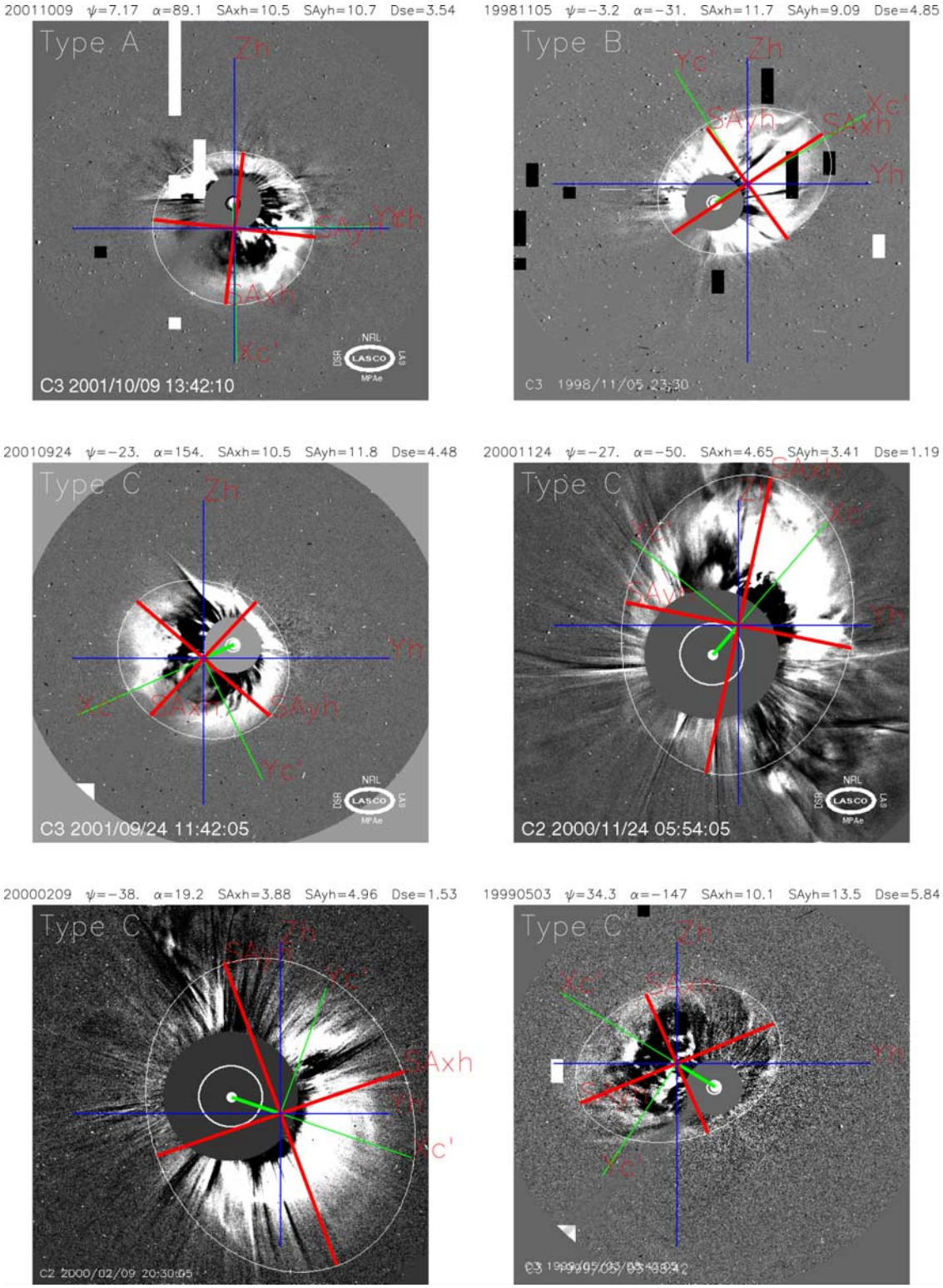

Figure 1. Definition of five halo parameters (SA_{xh}, SA_{yh}, ψ, D_{se}, and α) and Types A, B, and C for disk frontside full halo CMEs (see text for details). Here X'_c and Y'_c are, respectively, aligned with and perpendicular to the direction from the solar disk center to the halo center, D_{se} (the short thick green line). Parameters ψ and α denote the angles between SA_{yh} and Y'_c and between X'_c and Y_h, respectively.

nearly aligned with X'_c axis. The Type A halo may be formed by the circular or the elliptic cone model. The top right panel shows a sample of Type B halo where SA_{xh} denotes the semi major axis though it is nearly aligned with X'_c. The four events shown in middle and bottom rows are Type C halos. Both Type B and Type C halos certainly cannot be produced using the circular cone model, and their

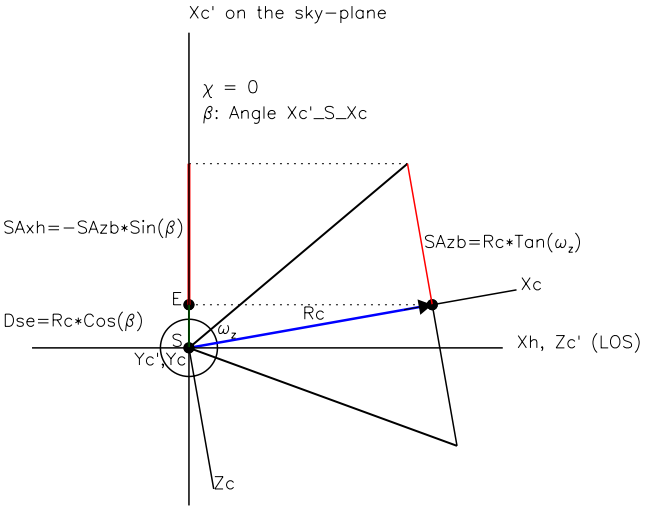

Figure 2. Three coordinate systems used in the transformation from the cone coordinate system $X_cY_cZ_c$ through the projection coordinate system $X_c'Y_c'Z_c'$ to the heliocentric ecliptic coordinate system $X_hY_hZ_h$. The projection of the elliptic cone base onto the sky-plane takes place from $X_cY_cZ_c$ to $X_c'Y_c'Z_c'$ and depends only on the parameter β, the angle from X_c to X_c'. The circle with a radius of 2 denotes the occulting disk of Coronagraph C2 on board SOHO.

model parameters must be inverted using the elliptic cone model.

[20] Among 30 events in Table 3 of *Cremades* [2005], the number of Types A, B, and C is 3, 7 and 20, respectively. This distribution implies that only 10% of disk FFH CMEs may be reproduced and inverted using the circular cone model. Since Type A halos may also be formed by the elliptic cone model as shown in sections 4 and 5, the model parameters inverted using the circular cone model for some Type A halos may significantly differ from the real ones.

3. Elliptic Cone Model and Model Parameters

[21] Since the shape of 3-D rope-like CME plasma structure may be better approximated using the elliptic cone model, halos formed on the sky-plane by Thompson scattering along the line-of-sight may be better reproduced by projecting the elliptic cone base onto the sky-plane.

3.1. Six Elliptic Cone Model Parameters: λ, ϕ, R_c, ω_y, ω_z, and χ

[22] As mentioned in section 1, the elliptic cone model is a hollow body which narrows to its apex from an elliptic, flat base. The position of an elliptic cone base in the heliocentric ecliptic coordinate system, $X_hY_hZ_h$, can be determined by locating the apex of the elliptic cone at the origin of the $X_hY_hZ_h$ system, and by specifying the direction of the central axis of the elliptic cone in the $X_hY_hZ_h$ with latitude λ and longitude ϕ. Here the X_h axis is aligned with the line-of-sight, pointing to the Earth; λ and ϕ are measured with respect to the ecliptic plane X_hY_h and the line-of-sight X_h, respectively.

[23] To define the size, shape and orientation of elliptic cone bases we introduce a "cone coordinate system," $X_cY_cZ_c$, and a "projection coordinate system," $X_c'Y_c'Z_c'$ (see Figure 2 for the definition of the three axes). As shown in Figure 2 and the left column of Figures 3 and 4, the distance between the base and apex is denoted by R_c, and the half angular widths corresponding to two semi-axes of the cone bases, SA_{yb} and SA_{zb}, are by ω_y and ω_z. As shown in the bottom panel of the left column of Figures 3 and 4, the angle, χ, between SA_{yb} and Y_c or between SA_{zb} and Z_c axes, specifies the orientation of the cone base. Therefore six model parameters are needed to characterize the location, the shape and size, and the orientation of the base of a 3-D elliptic cone model in the $X_hY_hZ_h$ system.

3.2. Relationship Between λ, ϕ and β, α

[24] As shown in Figures 1 and 2, the projection angle β, i.e., the angle between the central axis X_c and its projection on the sky-plane, X'_c, denotes the latitude of the central axis relative to the sky-plane, and the observed halo parameter α the longitude of the central axis relative to westward Y_h.

[25] The relationship between (β, α) and (λ, ϕ) is

$$\left\{\begin{array}{l}\sin\lambda = \cos\beta\sin\alpha\\ \\ \tan\phi = \cos\alpha/\tan\beta\end{array}\right\}\left\{\begin{array}{l}\sin\beta = \cos\lambda\cos\phi\\ \\ \tan\alpha = \tan\lambda/\sin\phi\end{array}\right\} \quad (4)$$

Equation (4) shows that parameter α (and β) depends on both λ and ϕ. Therefore the observed halo parameter α provides information of both λ and ϕ. This information will be used in finding out the unknown parameter β, as shown in section 5. It should be noted that positive angles are measured counterclockwise in rotation transformation.

[26] In fact, the projection of the elliptic cone base onto the sky-plane depends only on the projection angle, β. We will replace λ and ϕ by β in establishing the inversion equation system of the elliptic cone model.

3.3. Projection of the Elliptic Cone Base on the Sky-Plane

[27] Given a set of values for the five model parameters R_c, ω_y, ω_z, χ, β, a modeled halo on the plane $X_c'Y_c'$ can be obtained by the transformation of the rim of the elliptic cone base from coordinate system $X_eY_eZ_e$ to $X_cY_cZ_c$ and from $X_cY_cZ_c$ to $X'_cY'_cZ'_c$,

$$\begin{bmatrix}x'_c\\ y'_c\\ z'_c\end{bmatrix} = \begin{bmatrix}\cos\beta & -\sin\beta\sin\chi & -\sin\beta\cos\chi\\ 0 & -\cos\chi & -\sin\chi\\ \sin\beta & -\cos\beta\sin\chi & \cos\beta\cos\chi\end{bmatrix}\begin{bmatrix}x_{eb}\\ y_{eb}\\ z_{eb}\end{bmatrix} \quad (5)$$

$$\begin{bmatrix}x_{eb}\\ y_{eb}\\ z_{eb}\end{bmatrix} = \begin{bmatrix}R_c\\ R_c\tan\omega_y\cos\delta_b\\ R_c\tan\omega_z\sin\delta_b\end{bmatrix} \quad (6)$$

where the symbol δ_b is the angle of radii of an elliptic base relative to SA_{yb} axis and increase along the rim of the elliptic base from 0° to 360°.

[28] Using parameter α and equation (3), the modeled halo on the plane Y_hZ_h can be obtained.

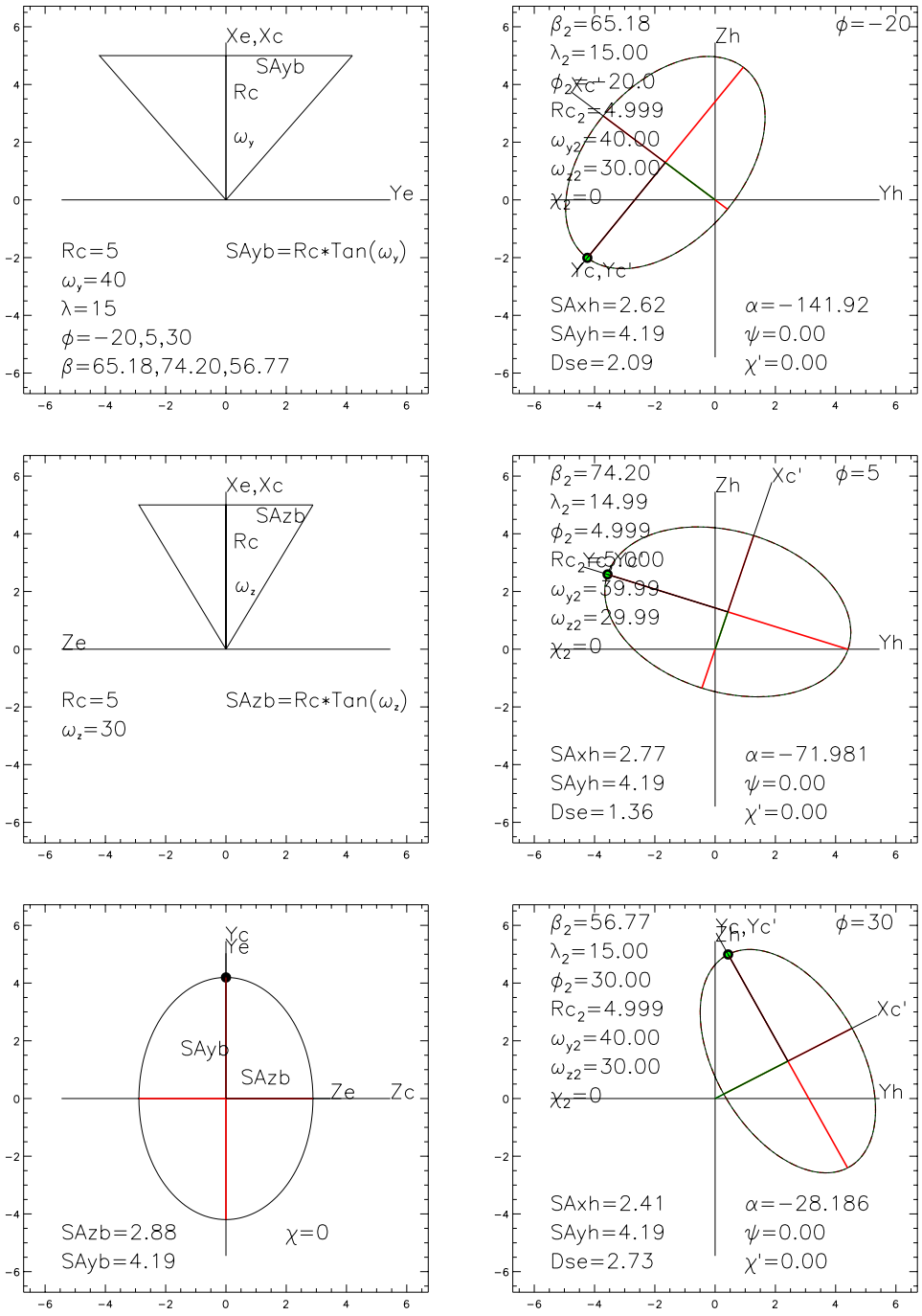

Figure 3. The left column shows the definition of elliptic cone model parameters R_c, ω_y, ω_z, and χ, and a set of values for six elliptic cone model parameters. The right column shows the three modeled halos (black ellipses) that are supposed to be observed by three spacecraft located on the ecliptic plane with different azimuths. The inverted model parameters with subscript "2" are also shown in each panel in the right column. The green and red dashed ellipses are modeled halos calculated using inverted elliptic and circular cone model parameters, respectively.

3.4. Modeled Halos

[29] Given a set of model parameters λ, ϕ, ω_y, ω_z, R_c and χ, as shown in the left column of Figures 3 and 4, we first calculate β and α using λ, ϕ and equation (4), then predict the elliptic halo on the sky-plane using equations (5), (6) and (3). The black ellipses in the right column of Figures 3 and 4 show the modeled halos that are expected to be observed by coronagraphs on board three spacecraft, say, STEREO A, SOHO, and STEREO B, simultaneously. As shown in each panel of the right column in Figures 3 and 4, the five halo parameters SA_{xh}, SA_{yh}, D_{se}, ψ, and α can be calculated on the basis of the modeled halos.

[30] The small green and big black dots in each panel denote, respectively, the semi axis of the modeled halos

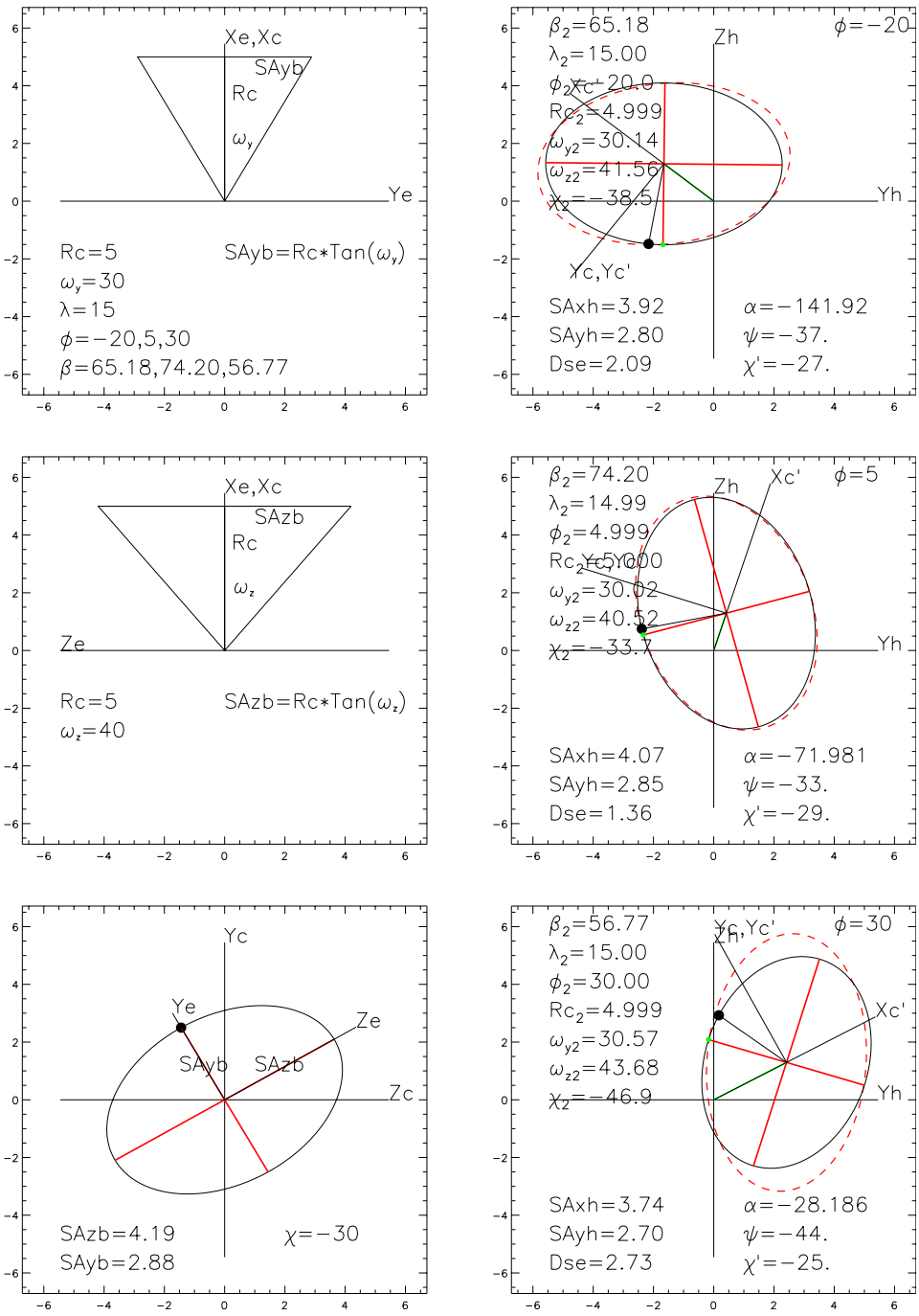

Figure 4. The same as Figure 3 but with different ω_y, ω_z, and χ, as shown in the left column.

located near the Y'_c axis and the projection of the base semi-axis SA_{yb} on the Y_hZ_h plane. Parameters ψ and χ' denote, respectively, the angular distance of the green and black dots from the Y'_c axis. The values of ψ and χ' in Figures 3 and 4 depend on χ and β. The difference $\chi' - \chi$ and $\psi - \chi$ show the effect of the projection. Both χ' and ψ are zero when $\chi = 0$ (see Figure 3).

4. Inversion Equation System and Its Solution

[31] In order to invert the unknown model parameters from observed halo parameters, we first establish the inversion equation system that relates model parameters with halo parameters. We then find out the solution of the inversion equation system.

4.1. Inversion Equation System of the Elliptic Cone Model

[32] The inversion equation system of the elliptic cone model may be established by comparing observed and modeled halos on the plane of $X'_cY'_c$. Equations (1) and (2) describe observed elliptic halos on the plane of $X'_cY'_c$ using four halo parameters SA_{xh}, SA_{yh}, D_{se}, ψ. Equations (5) and (6) are the expressions of modeled elliptic halos on the

same plane, but using five model parameters R_c, ω_y, ω_z, χ, and β.

[33] By comparing the like items between equations (1) and (5), and setting $\delta_h = \delta_b + \Delta\delta$, the relationship between elliptic cone model parameters and elliptic CME halo parameters can be established

$$\begin{aligned} R_c \cos\beta &= D_{se} \\ R_c \tan\omega_y \sin\beta \sin\chi &= SA_{xh} \cos\psi \sin\Delta\delta + SA_{yh} \sin\psi \cos\Delta\delta \\ -R_c \tan\omega_z \sin\beta \cos\chi &= SA_{xh} \cos\psi \cos\Delta\delta - SA_{yh} \sin\psi \sin\Delta\delta \\ R_c \tan\omega_y \cos\chi &= -SA_{xh} \sin\psi \sin\Delta\delta + SA_{yh} \cos\psi \cos\Delta\delta \end{aligned} \tag{7}$$

All model (halo) parameters occur in left (right) side of the equation system (7). By assuming $\Delta\delta = \delta_h - \delta_b \simeq \psi - \chi$, we have

$$\begin{aligned} R_c \cos\beta &= D_{se} \\ \left(R_c \tan\omega_y \sin\beta + a\right) \tan\chi &= b \\ -R_c \tan\omega_z \sin\beta - b \tan\chi &= a \\ R_c \tan\omega_y - b \tan\chi &= c \end{aligned} \tag{8}$$

where

$$\begin{aligned} a &= SA_{xh} \cos^2\psi - SA_{yh} \sin^2\psi \\ b &= \left(SA_{xh} + SA_{yh}\right) \sin\psi \cos\psi \\ c &= -SA_{xh} \sin^2\psi + SA_{yh} \cos^2\psi \end{aligned} \tag{9}$$

[34] For Types A and B FFH CMEs, $\psi = 0$ and $\chi = 0$, equation systems (8), (9) become

$$\begin{aligned} R_c \cos\beta &= D_{se} \\ -R_c \tan\omega_z \sin\beta &= SA_{xh} \\ R_c \tan\omega_y &= SA_{yh} \end{aligned} \tag{10}$$

and when $\omega_y = \omega_z$, the number of model parameters equals the number of halo parameters, equation system (10) reduce to the inversion equations for the circular cone model [*Xie et al.*, 2004].

[35] It is interesting to note that $D_{se} = R_c \cos\beta$, showing that halo parameter D_{se} depends on R_c and it increases as time increases. This time-dependent characteristic of D_{se} is determined by the cone apex located at Sun's spherical center (see Figure 2 and the left panels in Figures 3 and 4). There is a circular cone model that lays the apex of the cone model at the solar surface, instead of the spherical center of the Sun assumed here. For this kind of circular cone model, the parameter D_{se}, i.e., the distance between the solar disk center and the elliptic halo center, is a constant [*Michalek et al.*, 2003]. This different time variation of D_{se} may be used to determine which circular cone model should be selected to invert the circular cone model parameters for a specific Type A halo CME.

4.2. Solutions of the Inversion Equation System

[36] From equation system (8), we have

$$\begin{aligned} R_c &= D_{se} / \cos\beta \\ \tan\omega_y &= \frac{-(a - c\sin\beta) + \left[(a + c\sin\beta)^2 + (4\sin\beta b^2)\right]^{0.5}}{2R_c \sin\beta} \\ \tan\chi &= \left(R_c \tan\omega_y - c\right)/b \\ \tan\omega_z &= -(a + b\tan\chi)/R_c \sin\beta \end{aligned} \tag{11}$$

Equation system (11) shows that the four unknown model parameters in the left side can be calculated only when the model parameter β as well as the four halo parameters are given. For Types A and B when $\psi = 0$, equation system (11) becomes

$$\begin{aligned} R_c &= D_{se} / \cos\beta \\ \tan\omega_y &= SA_{yh}/R_c \\ \tan\omega_z &= -SA_{xh}/(R_c \sin\beta) \end{aligned} \tag{12}$$

The solution of three model parameters R_c, ω_y and ω_z are determined by the model parameter β and three halo parameters D_{se}, SA_{xh} and SA_{yh}. Expressions (11) and (12) show that as β increases, R_c increases, and ω_y and ω_z decreases when the halo parameters are given. It should be noted that the half angular width ω_z inverted here corresponds to the angle measured clockwise from X_c to the lower side of the cone (see Figure 2). In what follows we show only the inverted value, neglecting its sign. When $\omega_y = \omega_z$, equation system (12) becomes

$$\begin{aligned} \sin\beta &= SA_{xh}/SA_{yh} \\ R_c &= D_{se} / \cos\beta \\ \tan\omega &= SA_{yh}/R_c \end{aligned} \tag{13}$$

In this case, three model parameters (ω, R_c, β) can be uniquely determined by three halo parameters (SA_{xh}, SA_{yh}, D_{se}). Expression (13) is just the inversion solution of the circular cone model derived by *Xie et al.* [2004].

5. Determination of the Propagation Direction and Inversion Solution for Disk FFH CMEs

[37] As shown above, the number of unknown model parameters occurred in the solution expressions of the inversion equation system is always one more than the number of given halo parameters. The only way to obtain the unique inversion solution of the elliptic cone model is to specify the model parameter β as well as halo parameters. We have pointed out in section 3 that the given halo parameter α, that does not occur in the inversion equation system, contains the information of the model parameters ϕ and λ, and may be used to determine parameter β that depends on ϕ and λ.

[38] The following two approaches can be used to determine the central axis direction (or the propagation direction) of disk FFH CMEs. Once the parameter β is calculated, the inversion solution of R_c, ω_y, ω_z and χ can be calculated using (11) for Type C and (12) for Types A and B.

5.1. Two-Point Observation

[39] The parameter β can be determined by using two halo CME images observed at the same time by two spacecraft flying on the ecliptic plane. The three modeled halos in the right columns of Figures 3 and 4 are expected to be observed by STEREO A, SOHO, and STEREO B. Any two modeled CME halos provide two values of parameter α, say, α_a and α_b, that contain information of two sets of λ and ϕ for the CME propagation direction. The corresponding two spacecraft are located at the ecliptic plane with their azimuthal difference of $\Delta\phi$. The central axis direction of a CME viewed from any two spacecraft are (λ, ϕ_a) and (λ, $\phi_a + \Delta\phi$). Using equation system (4) we can easily calculate λ, ϕ_a and thus β. For instance, the two modeled halos in top right and middle right panels of Figure 3 show that $\alpha_a = -141.92°$, $\alpha_b = -71.981°$, and $\Delta\phi = 25°$, we obtain $\phi_2 = -20.0°$, $\lambda_2 = 15.00°$ and $\beta_2 = 65.18°$, as shown in the top right panel of Figure 3. They are exactly the same as the original values.

[40] Using such calculated projection angle β and the values of four given halo parameters D_{se}, SA_{xh}, SA_{yh} and ψ (see the top right panel of Figure 3), the model parameters R_c, ω_y, ω_z and χ can be calculated using equation systems (9) and (11). The parameters β_2, λ_2, ϕ_2, r_{c2}, ω_{y2}, ω_{z2}, and χ_2 shown in the top right panel of Figure 3 denote the inverted results. The results shown in middle right and bottom right panels are obtained using the same method for the middle and bottom cases. All three model validation experiments show that expressions (4) and (11) can be used to accurately invert the solution of elliptic cone model parameters for disk FFH CMEs with $\chi \simeq 0$. The red dashed ellipse is calculated using the inverted six model parameters. They completely agree with black ellipse.

[41] All three black ellipses in Figure 3 are Type A, and produced by the same elliptic cone but with different ϕ. In practice, it is difficult, if not impossible, to determine if a Type A disk FFH CME is formed by a circular or a elliptic cone. To see the difference of inverted circular cone model parameters from the original ones, we first calculate the circular cone model parameters using (13) and three halo parameters (D_{se}, SA_{xh}, SA_{yh}), and then produce the green dotted ellipses on the basis of the inverted model parameters. Although the green ellipses are also completely agree with the black ellipses, the obtained values for three circular cone model parameters are totally different from the original elliptic cone model parameters (see left column of Figure 3). For instance, the inverted circular cone model parameters for the top right panel are $R_c = 2.69$, $\omega_y = \omega_z = 57.36$, $\beta = 38.65$, and $\lambda = 28.79°$, and $\phi = -44.55°$. They are certainly not usable. This experiment shows that even for Type A disk FFH CMEs, it is not safe to use the circular cone model to invert the model parameter.

[42] Figure 4 is the same as Figure 3, but the values of ω_y ω_z and χ are different from Figure 3 (see the left column). The red dashed ellipses in the right column of Figure 4 are obtained using the same way as Figure 3 but their agreement with black ellipses is worse than Figure 3. Comparison of the inverted model parameters with the original ones show that the parameters λ, ϕ, R_c and ω_y agree with original ones very well; and dependent on β, the inverted ω_z is slightly different from original and the inverted χ may be significantly different from original.

5.2. One-Point Observation

[43] A CME can propagate in any direction (ϕ, λ) in the 3-D space. For a specified value of α, all possible sets of ϕ and λ are reduced from whole ϕ-λ plane to a specific curve, as shown in each panel of Figure 5. The six curves in Figure 5 correspond to the six values of α shown in Figure 1. These curves are obtained by assuming that the possible value of β for disk FFH CMEs ranges from 45° to 90°.

[44] To search for the optimum central axis direction (β or ϕ_{ce}, λ_{ce}) among all possible directions on a curve corresponding to a specific value of the halo parameter α, it is necessary to use additional information that is associated with the CME propagation direction or the center of CME source region.

[45] CME-associated flares or active regions are believed to be located near the center of CME source region [e.g., *Zhao and Webb*, 2003], though they are often located near one leg of CMEs [e.g., *Plunkett et al.*, 2001]. The dot in each panel of Figure 5 denotes the location of the CME-associated flare.

[46] Taking consideration the effect of interaction between higher-latitude high speed streams and lower-latitude CME in the declining and minimum phases of solar activity, it was suggested that the optimum propagation direction may be found by moving the flare location southwardly, i.e., by lowering the flare latitude while keeping the flare longitude constant [*Cremades*, 2005]. This approach cannot work for all cases shown in Figure 5, especially for the cases of top left and bottom left panels. In addition, this approach may not be working for all phases of solar activity.

[47] We find out the optimum central axis direction among all possible direction on a curve by finding out the minimum distance between the dot and the curve in each panel of Figure 5. The calculated β and (ϕ_{ce}, λ_{ce}) are shown in the southwest quadrant of each panel.

[48] It should be noted that the location of flares is often specified using the latitude and longitude measured in the heliographic coordinate system, i.e., the latitude and longitude measured with respect to the solar equator, instead of the solar ecliptic plane. The effect of B0 angle (the heliographic latitude of the Earth) should be corrected before finding out the optimum model parameter β. The symbols ϕ_{fs}, λ_{fs} and ϕ_{fe}, λ_{fe} denote longitude and latitude of CME-associated flares measured in the heliographic and the heliocentric ecliptic coordinate systems, respectively. We first calculate ϕ_{fe}, λ_{fe} using ϕ_{fs}, λ_{fs}, and $B0$, then find out ϕ_{ce}, λ_{ce} using ϕ_{fe}, λ_{fe} (the dot) and α (the curve).

[49] Once the optimum value of the projection angle β is obtained, the model parameters that are supposed to form the observed halos (white ellipses in Figures 6, 7, and 8) can be inverted using observed four halo parameters SA_{xh}, SA_{yh}, D_{se}, and ψ, as shown on the top of each panel in Figure 1. Figures 6, 7, and 8 display the calculated elliptic cone model parameters for the six disk FFH CMEs in Figure 1. The green ellipse in each panel of Figures 6, 7, and 8 is

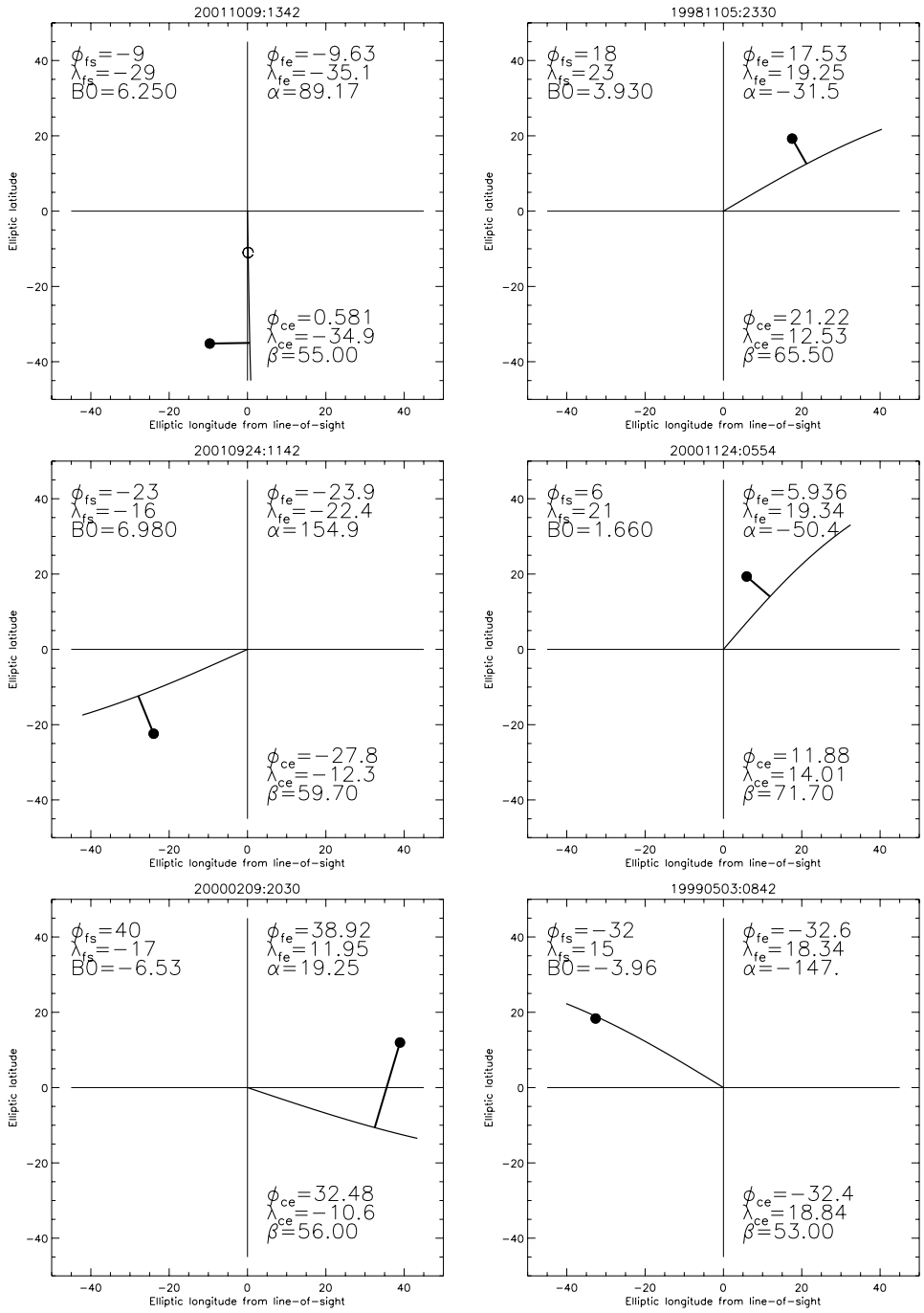

Figure 5. Description of the one-point approach for finding out the CME propagation direction (ϕ_{ce}, λ_{ce}) or β on the basis of halo parameter α and the location of CME-associated flare (ϕ_{fs}, λ_{se}). See text for details.

calculated from the inverted six model parameters and equation system (5), (6) and (3). The comparison of the green ellipses with the white ellipses show that the agreement between green and white ellipses depend on the parameters β and χ. When $\chi < 30°$ the agreement is reasonable, as shown in Figures 6 and 7. When inverted $\chi > 30°$ the difference increases as β decreases as shown in Figure 8. It is similar to what we find out from Figure 4. The similarity might suggest that the projection angle β obtained using one-point approach is acceptable.

[50] FFH CMEs of Types B and C can be fitted only by the elliptic cone model. Type A event, such as the 9 October 2001 event in the top panel of Figure 6, can be formed by projecting a circular or elliptic base onto the sky-plane, and thus can be fitted by the elliptic or circular cone model. As shown by Equations (12) and (13) when $\omega_y = \omega_z$, the inversion solutions obtained using circular and elliptic cone models should be the same if the real base is a circular one.

[51] To compare the inversion solutions of the elliptic cone model with that of the circular cone models, we fit the Type A halo of the 9 October 2001 using the circular cone

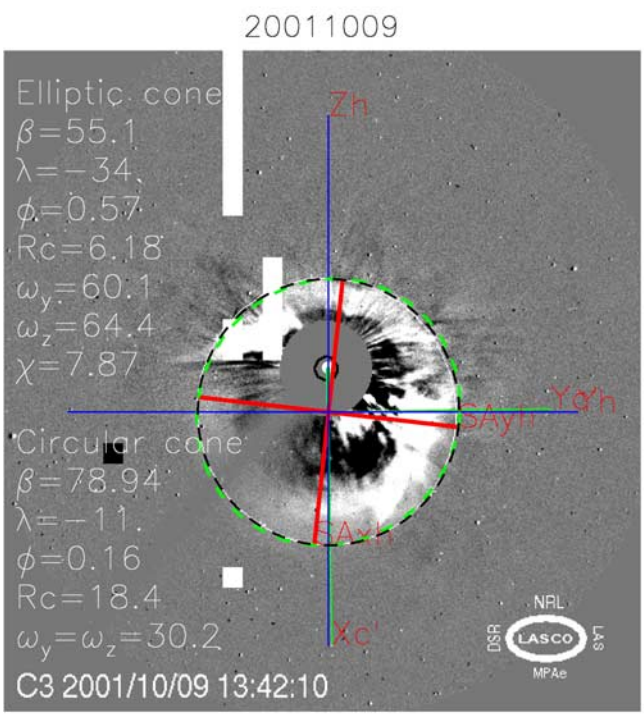

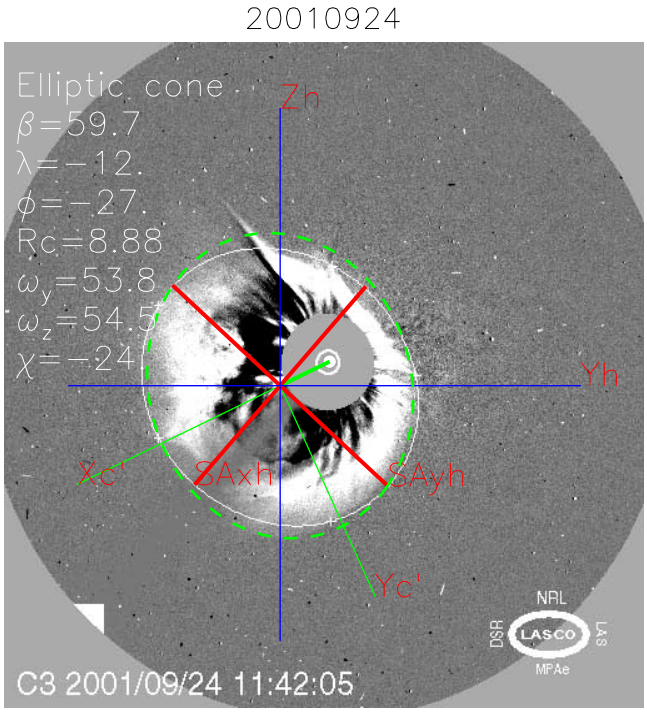

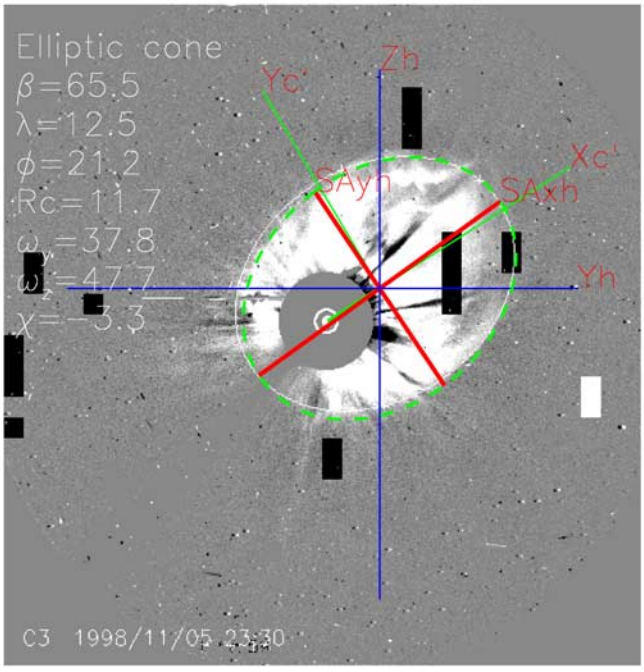

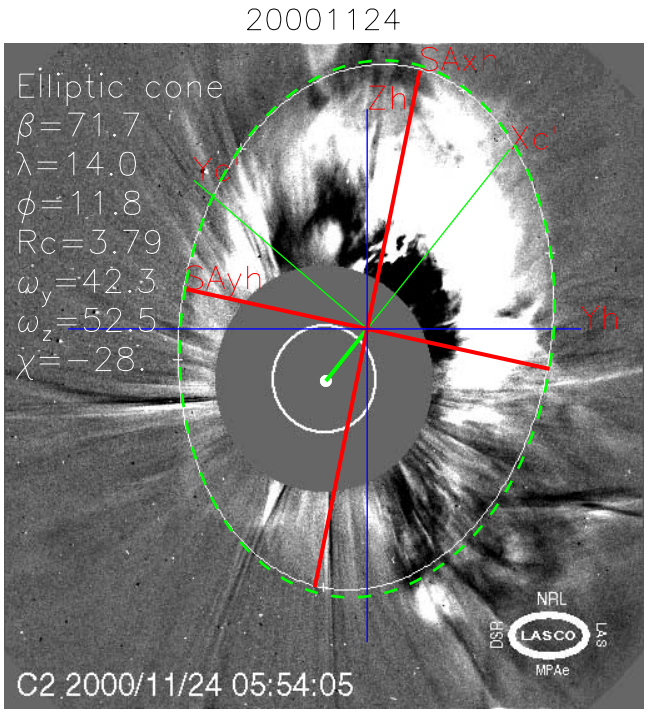

Figure 6. Elliptic and circular cone model parameters inverted using the halo parameters for the two halo events listed in the two top panels of Figure 1 and the parameter β inferred in the two top panels of Figure 4. The green and black dashed ellipses are calculated using the inverted elliptic and circular cone model parameters, respectively.

Figure 7. Elliptic cone model parameters inverted using the halo parameters for the two halo events listed in the two middle panels of Figure 1 and the parameter β inferred in the two middle panels of Figure 4. The green dashed ellipses are calculated using the inverted elliptic cone model parameters.

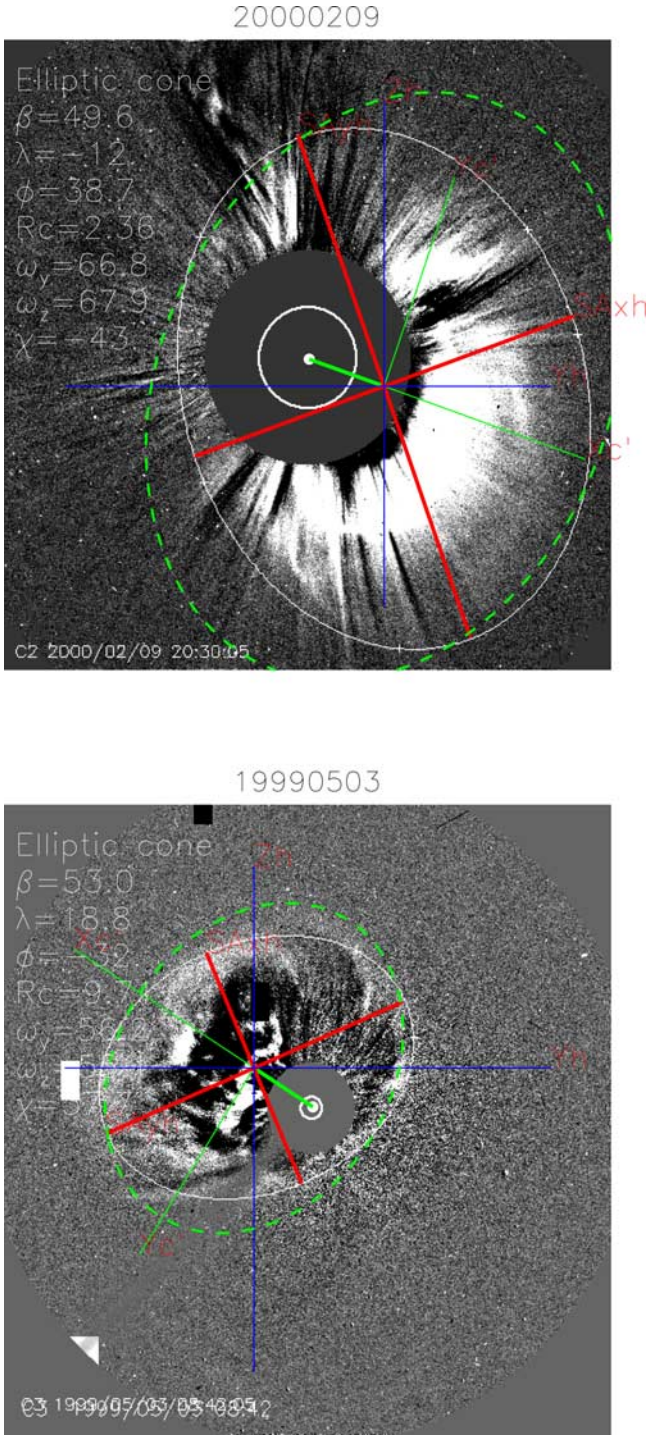

Figure 8. The same as Figure 7, but corresponding to the two halo events listed in the two bottom panels of Figure 1.

model as well as the elliptic cone model. Listed in the panel are the inverted circular cone model parameters as well as the inverted elliptic cone model parameters. The black dashed ellipse is obtained using the circular cone model parameters. Although the agreement of both the green and black ellipses with the observed white ellipse is equally well, the elliptic cone model parameters are significantly different from the circular cone model parameters. The central axial direction inverted from the circular cone model (the open circle in the top left panel of Figure 5) is located far from the CME-associated flare location (the black dot), and the distance from the solar center to the elliptic base, R_c = 18.4 solar radii, appears to be too far from the solar surface to produce observed brightness of the halo CME. Therefore the Type A halo of the 9 October 2001 event is caused by the elliptic cone model, instead of the circular cone model.

6. Summary and Discussions

[52] We have shown that on the sky-plane Y_h Z_h, disk FFH CMEs provide five halo parameters, and can be classified into Types A, B, and C, depending on the major axis of elliptic halos being perpendicular to, aligned with, or anywhere else from the direction from the solar disk center to the CME halo center.

[53] The elliptic cone model needs six model parameters to characterize its morphology in the heliocentric ecliptic coordinate system X_h Y_h Z_h.

[54] However, the morphology of the CME halo and the elliptic cone base in the projection coordinate system X_c' Y_c' Z_c' can be described by four halo and five model parameters, respectively. In the system X_c' Y_c' Z_c', the halo parameter α disappears, and the two model parameters λ and ϕ that denote the CME propagation direction in X_h Y_h Z_h are replaced by one new model parameter β, the projection angle.

[55] On the other hand, the axis Y_c' is the reference axis for measuring the orientation of both elliptic CME halos and elliptic cone bases. The inversion equation system of the elliptic cone model and its solution can thus be established by setting $\delta_h = \delta_b + \Delta\delta$, and assuming $\Delta\delta = \delta_h - \delta_b \simeq \psi - \chi$, and by comparing the like term in the expressions between modeled and observed halos in the X_c' Y_c' Z_c' system.

[56] The halo parameter α that does not occur in the inversion equation system depends on both latitude and longitude of the CME propagation direction (λ, ϕ), and has been used to estimate the model parameter β on the basis of two-point or one-point observations of halo CMEs.

[57] The two-point approach uses two values of α observed at the same time by COR1 and COR2 on board STEREO A and B. Model validation experiments have been carried out for the cases of $\chi = 0°$ and $\chi = -30°$. The experiment results show that the CME propagation direction can be accurately determined by the two-point approach. The other four model parameters can also be accurately inverted for the case of $\chi = 0°$, i.e., for Types A and B disk FFH CMEs. For the case of $\chi = -30°$, i.e., Type C disk FFH CMEs, the obvious difference occurs only between inverted and original parameter χ, the orientation of the elliptic cone base. These results imply that the difference is caused by the assumption of $\Delta\delta = \delta_h - \delta_b \simeq \psi - \chi$, that is made in establishing the inversion equation system (8).

[58] The one-point approach combines the value of α with such simultaneous observation as the location of CME-associated flare, which includes the information associated with CME propagation direction. The six events displayed in Figure 1 for showing the three types of disk FFH CMEs have been tested. Both the propagation direction obtained using one-point approach and the other four model param-

eters inverted appear to be reasonable and acceptable. The agreement between the observed halos and modeled halos depends mainly on the projection angle β. It is the same as what we find in the model validation experiments for the two-point approach. The STEREO data are expected to be used to finally determine in what extent the CME propagation direction obtained from the one-point approach is correct.

[59] After obtaining the elliptic cone model parameters, the CME propagation speed can be determined using the method similar to *Zhao et al.* [2002] or *Xie et al.* [2004].

[60] The inversion equation system of the elliptic cone model and the expression of its solution can be reduced to that of the circular cone model. For Type A modeled halos in Figure 3 and observed halos in Figure 6, three circular cone model parameters are also inverted on the bases of three halo parameters. Both results show significant differences from the inverted elliptic cone model parameters, though the modeled halos calculated using the circular cone model parameters completely agree with the observed halos.

[61] It is difficult, if not impossible, to distinguish halos produced by elliptic cone from that by circular cone. The circular cone model should be used with utmost care lest it leads to erroneous conclusions. The inverted elliptic cone model parameters should be the same as the inverted circular cone model parameters if the base of the cone-like CME structure is circular. It is suggested to use the elliptic cone model to invert the geometric and kinematic properties for all Type A disk FFH CMEs.

[62] There are some disk FFH CMEs that are not purely elliptic. Some of them may be formed by ice-cream cone models. It has been shown that by determining the halo parameters from the rear part of the asymmetric halos, the elliptic cone model presented here can still be used to invert the model parameters for these asymmetric disk FFH CMEs (X. P. Zhao, Ice cream cone models for halo coronal mass ejections, manuscript in preparation, 2008).

[63] The accuracy of inversion solutions depends significantly on the halo parameters measured from observed disk FFH CMEs. We have developed codes to calculate the five halo parameters on the basis of the outer edge of halo CMEs. All the white elliptic outer edge shown in Figure 1 were determined using the five-point technique (see *Cremades* [2005] for details). To further improve the accuracy of the halo parameters we plan to automatically and more objectively recognize the outer edge of disk FFH CMEs using the pattern or feature recognition technique.

[64] **Acknowledgments.** We thank H. Cremades for sending us her Ph.D. thesis and her data product for 30 disk FFH CMEs. The six images in Figure 1 are selected from the 30 disk FFH CMEs. This work is supported by NASA grants NAGW 2502 and NAG5-3077 and by NSF grant ATM9400298.

[65] Amitava Bhattacharjee thanks David Webb and Gang Li for their assistance in evaluating this paper.

References

Cremades, H. (2005), Three-Dimensional Configuration and Evolution of Coronal Mass Ejections, Ph.D. thesis, Copernicus, Katlenburg-Lindau, Germany.

Cremades, H., and V. Bothmer (2005), Geometrical properties of coronal mass ejections, in *Coronal and Stellar Mass Ejections: Proceedings of IAU Symposium 226*, edited by K. P. Dere, J. Wang, and Y. Yan, pp. 48–54, Int. Astron. Union, Paris.

Gopalswamy, N., A. Lara, S. Yashiro, S. Nunes, and R. A. Howard (2003), Coronal mass ejection activity during solar cycle 23, in *Proceedings of the ISCS 2003 Symposium on Solar Variability as an Input to Earth's Environment*, *Eur. Space Agency Spec. Publ.*, *ESA-SP 535*, 403–414.

Gopalswamy, N., S. Yashiro, and S. Akiyama (2007), Geoeffectiveness of halo coronal mass ejections, *J. Geophys. Res.*, *112*, A06112, doi:10.1029/2006JA012149.

Howard, R. A., D. J. Michels, N. R. Sheeley Jr., and M. J. Koomen (1982), The observation of a coronal transient directed at Earth, *Astrophys. J.*, *263*, L101–L104.

Michalek, G., N. Gopalswamy, and S. Yashiro (2003), A new method for estimating widths, velocities, and source location of halo coronal mass ejections, *Astrophys. J.*, *584*, 472–478.

Odstrcil, D., and V. J. Pizzo (1999), Distortion of the interplanetary magnetic field by three-dimensional propagation of coronal mass ejections in a structured solar wind, *J. Geophys. Res.*, *104*(A12), 28,225–28,240.

Odstrcil, D., P. Riley, and X. P. Zhao (2004), Numerical simulation of the 12 May 1997 interplanetary CME event, *J. Geophys. Res.*, *109*, A02116, doi:10.1029/2003JA010135.

Plunkett, S. P., et al. (2001), Solar source regions of coronal mass ejections and their geomagnetic effects, *J. Atmos. Sol. Terr. Phys.*, *63*, 389–402.

Riley, P., C. Schatzman, H. V. Cane, I. G. Richardson, and N. Gopalswamy (2006), On the rates of coronal mass ejections: Remote solar and in situ observations, *Astrophys. J.*, *647*, 648.

Sheeley, N. R., Jr., W. N. Hakala, and Y.-M. Wang (2000), Detection of coronal mass ejection associated shock waves in the outer corona, *J. Geophys. Res.*, *105*(A3), 5081–5092.

Xie, H., L. Ofman, and G. Lawrence (2004), Cone model for halo CMEs: Application to space weather forecasting, *J. Geophys. Res.*, *109*, A03109, doi:10.1029/2003JA010226.

Zhao, X. P. (2005), Determination of geometrical and kinematical properties of frontside halo coronal mass ejections, in *Coronal and Stellar Mass Ejections: Proceedings of IAU Symposium 226*, edited by K. P. Dere, J. Wang, and Y. Yan, pp. 42–47, Int. Astron. Union, Paris.

Zhao, X. P., and D. F. Webb (2003), Source regions and storm effectiveness of frontside full halo coronal mass ejections, *J. Geophys. Res.*, *108*(A6), 1234, doi:10.1029/2002JA009606.

Zhao, X. P., S. P. Plunkett, and W. Liu (2002), Determination of geometrical and kinematical properties of halo coronal mass ejections using the cone model, *J. Geophys. Res.*, *107*(A8), 1223, doi:10.1029/2001JA009143.

X. P. Zhao, W. W. Hansen Experimental Physics Laboratory, Stanford University, Stanford, CA 94305-4085, USA. (xuepu@sun.stanford.edu)